Simulation of Two Rival Input Coupler Designs for the Superconducting Kaon Separator Cavity

C. Deibele, T. Berenc, M. Champion, J. Reid

Abstract: *The superconducting cavity for the kaon separator is being designed and built at FNAL. Two rival designs for the input coupler have been investigated and results presented. The fundamental difference between each design is the size of the diameter of the beampipe between the cavity resonator and the input coupler itself. The metric for determining a successful input coupler design is its ability to achieve a variety of loaded quality factors (Q_L) below the threshold of* 6×10^7.

I. Introduction and Numerical Considerations

Two fundamentally different designs for the input coupler were considered for the superconducting cavities for the kaon separator at FNAL. Each cavity, depicted schematically in Fig. 1, is a thirteen cell structure, and the cavity is operated in a dipole mode having a resonant frequency around 4 GHz. For system stability, it is desired that the cavity and coupler have a Q_L on the order of 6×10^7, which gives a bandwidth of

$$\Delta f = \frac{f_o}{Q_L} = \frac{4\times10^9\,Hz}{6\times10^7} = 66Hz.$$

Having a bigger bandwidth makes the design criteria for the control system of the resonant cavity cheaper and easier to make. Problems with a low bandwidth are, but not limited to, microphonics, phase lock loop, and tuning control. The numerical results contained in this

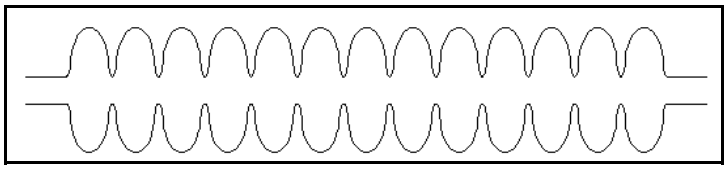

Figure 1. Schematic diagram of the final 13 cell kaon separator cavity. The input coupler would be, for example, on the right side of the cavity.

paper were calculated using the methods outlined by Berenc and Deibele[1] by Ginzton[2], and Slater[3]. Each result obtained in this paper was found by first simulating the cavity using the frequency-domain FEM code HFSS[4]. The simulated reflection measurement results were then exported then to a Mathcad[5] worksheet where it was analyzed.

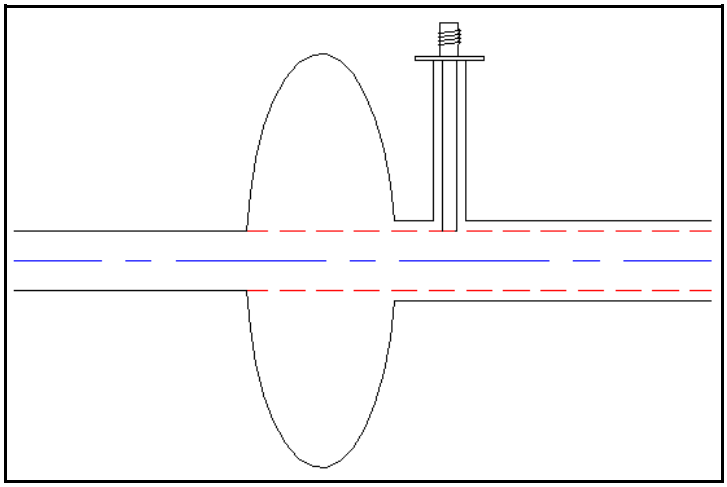

Figure 2. A 30 mm beampipe is on the left side of the cavity, and the coupler is connected to a 40 mm beampipe on the right side of the cavity. The feature of this coupler is that the coupler can penetrate into the beampipe and thereby increase coupling. The line leading into the cavity is assumed to be 50Ω, though by design, the coupler is designed to not be matched and this requirement can be easily relaxed.

The rival designs shown in this paper are depicted in Figs. 2-5. The major differences in the designs are the size of the beampipe on the coupler side of the cavity, although different geometries of antennas are analyzed. Featured in Fig. 2 is a cavity resonator with beampipes on each side of the cavity. The cavity has

---

[1]T. Berenc, C. Deibele, "Simulation and Measurement Considerations for Resonant Cavity Couplers and Extrapolating Results to Multiple Cells and Varying Conductivities," RFI Note #005, http://www-rfi.fnal.gov/technotes/TN/TN005.pdf.

[2]E.L. Ginzton, "Microwave Measurements," Mc-Graw-Hill Book Co., 1957, Library of Congress Catalog Number 56-13393.

[3]J. C. Slater, "Microwave Electronics," D. Van Nostrand Company Inc., 1950.

[4]HFSS, or High Frequency Structure Simulator is a program written by Ansoft corporation. Visit http://www.ansoft.com for more information.

[5]Mathcad is a program written by Mathsoft. For more information, visit http://www.mathsoft.com.

a 30mm beampipe on the left side of the cavity and a 40mm beampipe on the right side of the cavity. The 40mm section is added to increase the coupling into and out of the cavity. The red line in Fig. 2 is an extension of the 30mm diameter from the left side of the cavity. It is envisioned that the beam will have a diameter of circa 30mm, and therefore it is not permitted to penetrate further into the beampipe past this diameter.

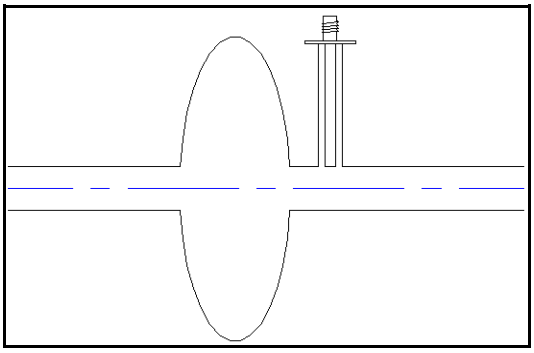

Figure 3. The antenna is again simulated assuming that its transmission line is 50Ω. The beampipes are 30 mm on each side of the cavity. The maximum penetration of the coupler is flush with the beampipe wall and is therefore an aperture type of coupler.

The next geometry that was investigated in this paper is shown in Fig. 3. Since the antenna is not permitted to penetrate past the beampipe wall, this method of coupling is similar to an aperture-type of coupling. This coupling is limited since it does not allow the antenna to penetrate into the beampipe. Its performance could be enhanced if the region between the cavity and the coupler would be opened or flared slightly and allow the fields between the coupler and cavity to interact. This will be discussed further in the results section of this paper.

The final types of couplers that will be addressed in this paper are off-axis couplers. Schematics of this type of coupler is depicted in Figs. 4 and 5. It was desired to analyze this type of coupler to increase the coupling from the schematic shown in Fig. 3 and demonstrate the aperture coupling of the antenna. The salient difference between the schematic of Fig. 4 and of Fig. 5 is a small washer-like piece of conductor placed at the end of the antenna. This conductor will shield fields on the opposite side of the antenna from the beampipe thereby increasing coupling.

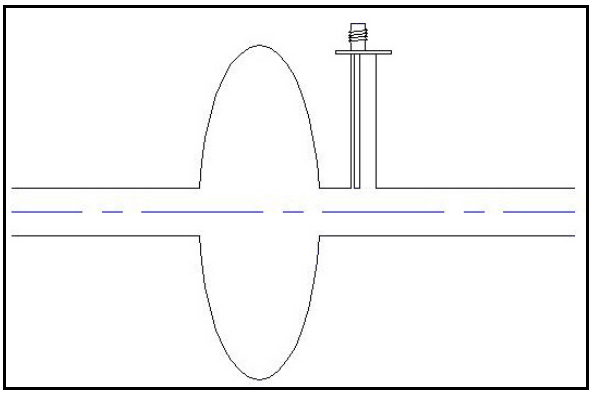

Figure 4. The antenna is off axis, and is matched to 50Ω.

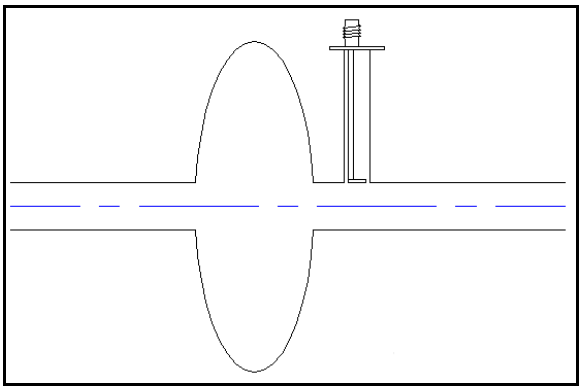

Figure 5. The same transmission line as in Fig. 4, but has a small pancake section on the end of the antenna. A picture of the antenna is shown in Fig. 12.

The transmission line leading into the cavity for all the designs that are considered in this paper is assumed to be 50Ω. This design requirement is not essential to the operation of the cavity since the cavity coupler is assumed to be run in a condition where it is overcoupled. Since the coupler, by definition, is not matched, it is possible that a short microwave matching section can be added to match to the characteristic impedance of the coupler transmission line and allow the impedance of the coupler be another free parameter to achieve optimum performance. This extra parameter was not examined in this paper and should be examined thoroughly for a more robust design.

II Numerical Considerations

A consideration which arises is the sensitivity of the estimation technique to the linear expansion of the reflection coefficient. The data that was collected in this analysis is calculated at discrete frequency points, and then the final results can be calculated by a linear interpolation. For example,

$$s_{11}(f) = \sum_{j=0}^{N-1} \theta\left(f, f_j, f_{j+1}\right)\left[\frac{\Gamma_{j+1} - \Gamma_j}{f_{j+1} - f_j}\left(f - f_j\right) + \Gamma_j\right] \qquad (1)$$

where

$$\theta\left(f, f_j, f_{j+1}\right)=\begin{cases}0 & f < f_j \\ 1 & f_j \le f \le f_{j+1}, \\ 0 & f > f_{j+1}\end{cases}$$

the set of f_j's are the discrete frequency points used in the calculation, and the set of Γ_j are the calculated reflection coefficients at each f_j. Using this technique, one can construct a piecewise linear function from the set of calculated reflection coefficients described by Eq. 1.

Using the formalism described in Eq. 1, it is desired to understand the limitations of the interpolation procedure. Using transmission line theory (assuming that the characteristic impedance of the transmission is normalized to one), we see that

$$\tilde{z}=\frac{1+\tilde{\Gamma}}{1-\tilde{\Gamma}}.$$

Using standard perturbation analysis, we can define the following parameter $\Delta\Gamma$:

$$\Gamma_{j+1}=\Gamma_j+\Delta\Gamma \quad \Rightarrow \quad \tilde{z}=\frac{1+\Gamma_j+\frac{\Delta\Gamma}{2}}{1-\Gamma_j-\frac{\Delta\Gamma}{2}}.$$

where $O(\Gamma)=1$, and $O(\Delta\Gamma)=O(\epsilon)$. After rewriting this, we see that

$$\tilde{z}=z_j\left(1+\frac{\Delta\Gamma}{2\left(1+\Gamma_j\right)}\right)\left(1-\frac{\Delta\Gamma}{2\left(1-\Gamma_j\right)}\right)^{-1}, \tag{2}$$

The final result is

$$\frac{\Delta\tilde{z}}{\tilde{z}}\cong\frac{\Delta\Gamma}{\left(1+\Gamma\right)^2}\left(1+\frac{\Delta\Gamma}{4}\right).$$

The analysis in [1] assumes that the set of frequency points is dense enough such that the constructed interpolated function is smooth. But even in this case, it is possible that for a strongly undercoupled antenna, $\frac{\Delta z}{z}$ can grow seemingly without bound. This is because for an

undercoupled antenna, by definition, Γ will be close to -1 because the reflection data is rotated to the detuned short position. In this case, it may be necessary to interpolate the impedance data rather than the reflection data.

An additional numerical error associated with the interpolation technique occurs when $\beta \approx 1$. An examination of Fig. 6 shows the data that was used in the analysis for the data in Table V-4. The calculation of the delay for this data resulted in a Smith chart shown in Fig. 7. This circle is not centered correctly about the detuned short position, and this will cause additional numerical errors with the estimate. Unfortunately, it is also not possible to use the resonant data point number 406 in this calculation either, since it would shift the resonant circle to another place along the circumference of the Smith chart. The final conclusion to this dilemma is that it is either necessary to fit a circle to the Smith chart data and to find the resonance from the fitted circle, or it is necessary to average results from the frequency points above the resonant frequency with the frequency points below the resonant frequency, and use the results that make the most sense. This

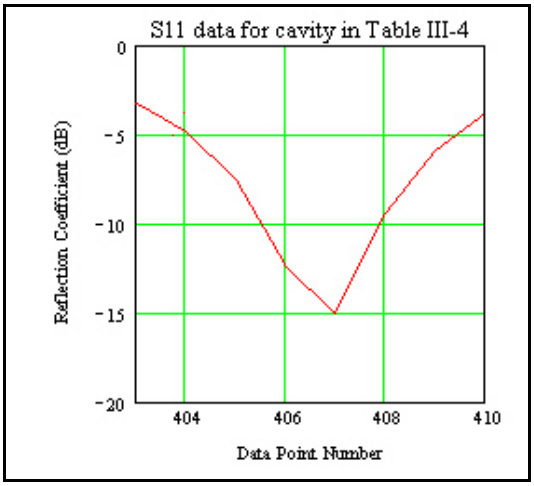

Figure 6. The resonance is assumed to be data point number 407. The cavity is nearly critically coupled.

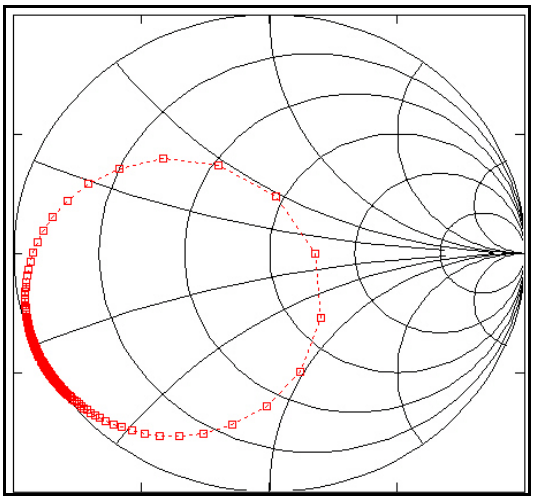

Figure 7. The appropriate delay is added to the datapoint #407 in Fig #6. The detuned short position is incorrectly found since the resonant frequency is not correct.

technique requires experience with the cavity and coupler of interest however.

IV. Simulation Results - 30mm Beampipe

The data in Table IV-1 was produced simulating the structure depicted in Fig. 8. The probe is flush with the beampipe so that it cannot intercept any beam in the beampipe. The transmission line is matched to 50Ω. The predicted results in Table IV-I show similarity to the results discussed in Table IV-3.

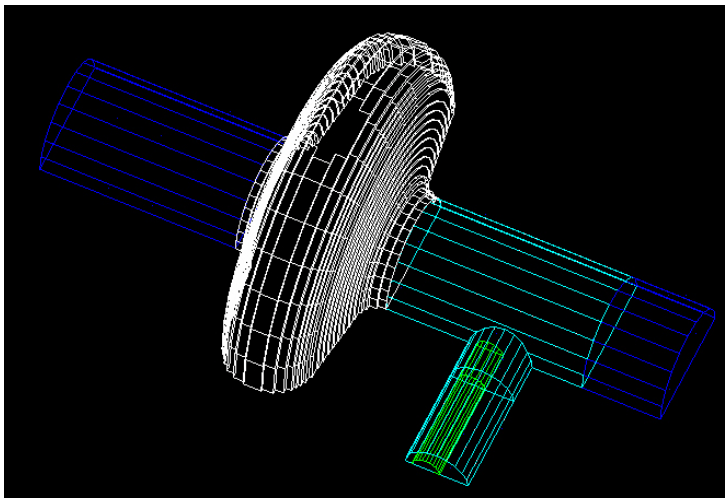

Figure 8. The cavity is depicted in white, and 30 mm beampipes are attached to each side of the cavity. A single probe is used to excite the cavity. The white and light blue sections are meshed with tetrahedra no greater than 5 mm per side, while the dark blue regions are meshed with tetrahedra no greater than 15 mm per side. The conductor is 65% the diameter of on-axis coax.

Table IV-1. Antenna is off axis, and the diameter of the antenna 65% the diameter compared to the on-axis antenna. This corresponds to the measurement schematic shown in Figs. 4 and 8. (β=0.046).

Parameter / Method	Q_o	Q_{ext}	Q_L	13 cell Nb Q_L
Q_{ext}	117928	2556380	112728	33122872
Q_L	118093	2559963	112886	33169146
Q_o	117909	2555968	112710	33117544
Average	117977	2557437	112774	33136520

The next geometry simulated was a structure depicted in Fig. 9. The structure shown in Fig. 9 is an on-axis transmission line of characteristic impedance of 50Ω. The transmission line is 2mm short of the 30mm beampipe, and a small piece of circular conductor, of thickness 2mm is added to the end of the transmission line. This small piece is often times termed the “hat”,

while the transmission line is commonly called a “plunger.” Again, the cavity resonator is the white structure and is meshed to 5mm as the maximum length on each tetrahedra. The coupling antenna is green in color. The mesh in the light blue area near the antenna is also set to a maximum of 5mm on each edge of every tetrahedra. The coupling does, as is expected, increase from the problem that does not have the hat at the end of the plunger. The coupling barely reaches the design goal however and therefore other geometries are explored. The results of the simulation are shown in Table IV-II.

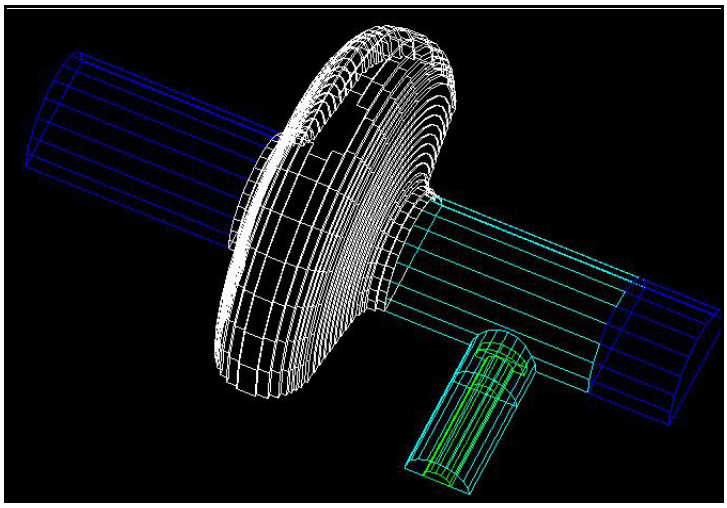

Figure 9. Cavity resonator with an on-axis feed-in transmission line of 50Ω. A 2 mm thick piece of conductor is added to the antenna to increase coupling.

Table IV-2. Antenna is on axis and has a small piece of circular conductor attached to the end of the antenna. This corresponds to the measurement schematic shown in Fig. 9. (β=0.049).

Parameter / Method	Q_o	Q_{ext}	Q_L	13 cell Nb Q_L
Q_{ext}	109318	2230940	104212	28918352
Q_L	108707	2218454	103629	28756970
Q_o	109415	2232918	104304	28943919
Average	109146	2227437	103928	28873080

The next geometry that will be examined is shown in Fig. 10 or in Fig. 3. The transmission line driving the cavity is 50Ω, and is axially concentric with the outer conductor of the transmission line driving the cavity. The antenna, or green part of Fig. 10, is flush with the 30mm beampipe. The cavity is meshed with a 5mm longest length tetrahedra. The driving line

is meshed with a 5mm longest length tetrahedra. The data is presented in Table IV-3. The similarity of data between Table IV-1 and Table IV-3 show that it a simple E-probe antenna that is flush with the beampipe is an effective aperture-type coupler and is limited as such.

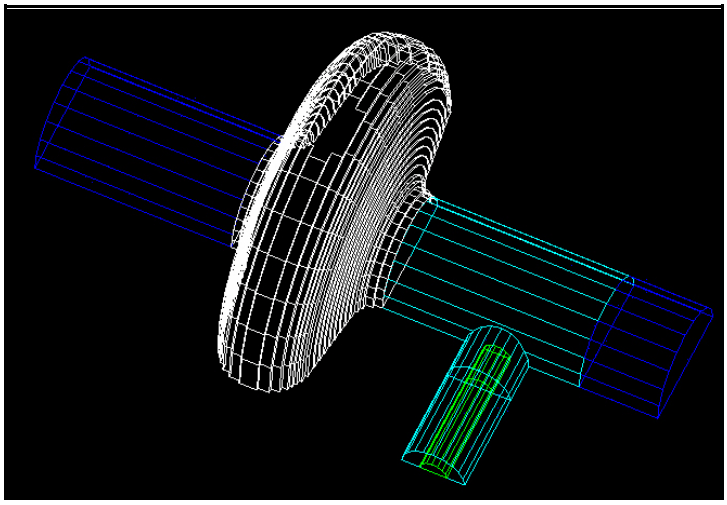

Figure 10. The on-axis dual of Fig. 8. The antenna penetration is flush with the beampipe. Notice that the coupling is similar between the two scenarios.

Table IV-3. Antenna is on axis. This corresponds to the measurement schematic shown in Fig. 10. (β=0.043).

Parameter / Method	Q_o	Q_{ext}	Q_L	13 cell Nb Q_L
Q_{ext}	99962	2307884	95812	29912752
Q_L	116612	2692282	111771	34877599
Q_o	117430	2711169	112555	35121421
Average	111335	2570447	106712	33303924

The next series of calculations that are presented are depicted in Figs. 5 & 11. The antenna is constructed by placing the antenna off-axis and matching it to 50Ω. A small hat was placed at the end of the antenna such that the hat is concentric with the outer conductor of the transmission line. A picture of two sample antennas are shown in Fig. 12. In Fig. 12, we see that N-connectors are used to transmit energy into the test cavity. While measurement data is not presented in this paper, the exact method of transferring energy into the cavity is essential for a good electrical match and robust design. Notice that the diameter of the hat for the antenna on

the left is greater than for the antenna on the right. This is because the off-axis displacement for the 50% diameter antenna is much greater than the off-axis displacement of the 65% antenna. The mathematics for determining the radius and position of the transmission line is covered in Appendix A.

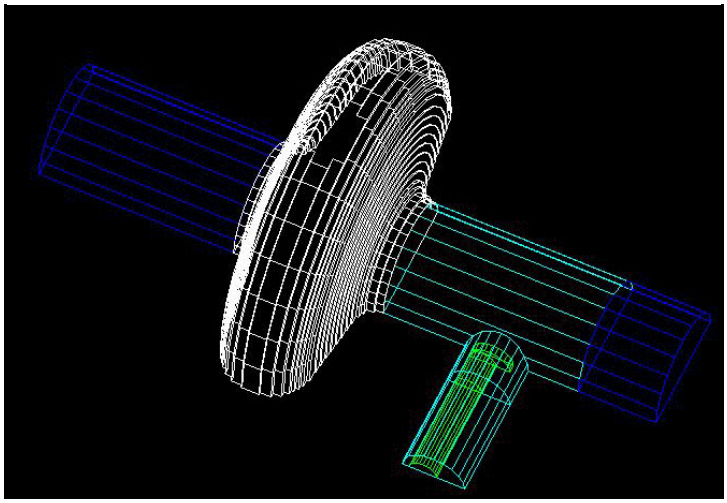

Figure 11. The transmission line is off-axis and has a circular "hat" on the end. The line is matched to 50Ω. The "hat" is placed on-axis and the left side of the "hat" is flush with the incoming transmission line.

The coupling increases for the case of Fig. 11 over the case of Fig. 9 because the coupling is aperture dominant. The theory, therefore, is explained by an integral equation. The integral equation is the same integral equation which is used to solve finite element electromagnetic problems. Finite element electromagnetic problems are solved by replacing free space with small regions of space surrounded by perfect conductor. Flowing on the surface of the conductor are electric and magnetic currents. When the currents are known then the fields internal to the perfect conductor are known. This

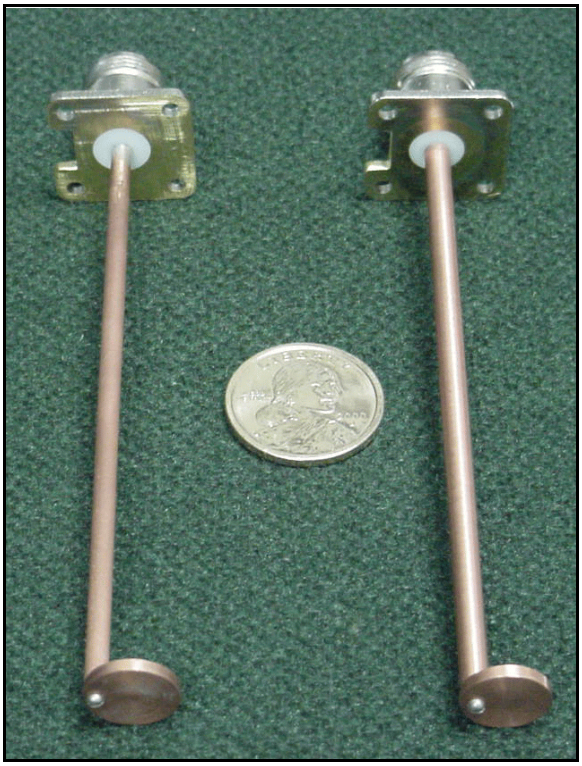

Figure 12. Two antennas used to excite a test cavity. The antenna on the left has a diameter that is 50% of an on-axis antenna, while the right-hand antenna is 65%.

problem is a classic problem and has been outlined by several authors. One author that does a good job explaining this equation is Harrington[6].

So, using the theory outlined by Harrington, we can replace the vacuum part of the aperture by perfect conductor and allow currents to flow on them. These currents therefore perform the coupling. The equation which does the coupling is then:

$$\vec{H}_{surface} = \oint_{surface} \vec{E} \times \hat{n} K\left(surface\right) ds$$

In this equation, since the driving electric field is radial in nature to the driving TEM line, and K is the greens function of the beampipe and does not vary along the length of the beampipe or azimuthally for the mode of interest, shielding a portion of the electric field will increase the coupling. It was chosen to shield the region away from the cavity resonator to take advantage of the natural evanescence of the beampipe modes.

One can see that the coupling then goes up by a factor of two using the shielded off axis probes. Having the shielding allows the design the be conservative. The design is not robust however because the best coupling is found when the antenna can penetrate past the beampipe wall and to disrupt the aperture coupling. This is discussed in Section V. Another method of coupling that should be addressed is waveguide coupling. Using the dominant $TE_{1,0}$ mode of a rectangular waveguide can also do excellent coupling and based on a simple geometry, it can be easily tunable with a movable aperture located within away from the beampipe. This is a big advantage to this method of coupling since the tuner could be placed in a warm region. It also is accommodates a less lossy mode to transfer energy into the cavity, which is of interest for the

---

[6]R.F. Harrington, "Time Harmonic Electromagnetic Fields," Mc-Graw Hill Book Co, 1961.

kaon separator project since the coax that is used now is lossy and can be a limiting factor in field levels that can be excited in the cavity resonator. The final advantage to using waveguide are the vacuum issues that are easily overcome using waveguide. Doing a study on couplers investigating waveguide coupling can show some interesting and most importantly project impacting results.

Table IV-4. Antenna is off axis, diameter is 65% that of the on-axis antenna, and has a small piece of circular conductor attached to the end of the antenna. This corresponds to the measurement schematic shown in Figs. 5 & 11. (β=0.113).

Parameter / Method	Q_o	Q_{ext}	Q_L	13 cell Nb Q_L
Q_{ext}	113653	1007053	102127	13074584
Q_L	114199	1011889	102618	13137286
Q_o	113595	1006536	102075	13067881
Average	113816	1008493	102273	13093250

Table IV-5. Antenna is off axis, diameter is 75% that of the on-axis antenna, and has a small piece of circular conductor attached to the end of the antenna. This corresponds to the measurement schematic shown in Figs. 5 & 11. (β=0.093).

Parameter / Method	Q_o	Q_{ext}	Q_L	13 cell Nb Q_L
Q_{ext}	113240	1212897	103570	15742844
Q_L	113419	1214820	103734	15767769
Q_o	113510	1215786	103817	15780282
Average	113390	1214501	103707	15763632

V. Simulation Results - 40 mm Beampipe

The profile of a single cell cavity was simulated. The cavity geometry that was simulated is shown in Fig. 9. The penetration of the center conductor of the antenna was varied to ensure that a full range of Q_L could be observed. The results are as follows:

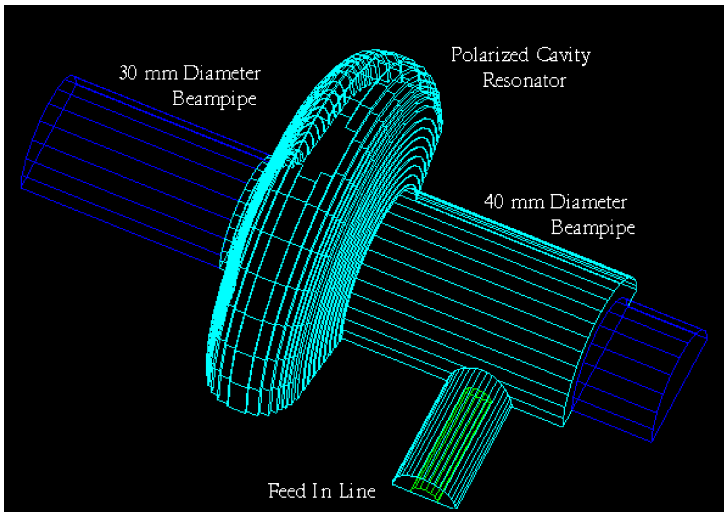

Figure 13. Cavity and coupler used to simulate the coupler connected to a 40 mm beampipe. This figure is used for the data in Tables V-1 to V-4. The data in Table V-5 has a small "hat" on the end, similar to the picture of Fig. 9.

Table V-1. Antenna penetrates to the 30mm diameter. This corresponds to the measurement schematic shown in Figs. 2 & 9. (β=10.424)

Parameter / Method	Q_o	Q_{ext}	Q_L	13 cell Nb Q_L
Q_{ext}	116022	11129	10155	144685
Q_L	115949	11122	10149	144594
Q_o	114481	10982	10020	142764
Average	115484	11078	10108	144014

Table V-2. Antenna penetrates to the 30mm diameter - 2mm. This corresponds to the measurement schematic shown in Fig. 2 & 9. (β=4.036)

Parameter / Method	Q_o	Q_{ext}	Q_L	13 cell Nb Q_L
Q_{ext}	114802	28444	22796	369761
Q_L	114702	28419	22776	369440
Q_o	112573	27892	22353	362584
Average	114026	28251	22642	367262

Table V-3. Antenna penetrates to the 30mm diameter - 4mm. This corresponds to the measurement schematic shown in Figs. 2 & 9. (β=3.944)

Parameter / Method	Q_o	Q_{ext}	Q_L	13 cell Nb Q_L
Q_{ext}	114883	29128	23237	378661
Q_L	114889	29130	23238	378681
Q_o	112288	28470	22712	370108
Average	114020	28910	23062	375817

Table V-4. Antenna penetrates to the 30 mm diameter - 6mm. This corresponds to the measurement schematic shown in Figs. 2 & 9. (β=1.432) Note the irregularities or variance in each estimate.

Parameter / Method	Q_o	Q_{ext}	Q_L	13 cell Nb Q_L
Q_{ext}	103297	72148	42478	937837
Q_L	79887	55797	32851	725311
Q_o	96441	67359	39659	875595
Average	116215	65101	38329	846247

Table V-5. Antenna penetrates to the 30 mm diameter with a 2 mm “pancake” on the end to increase coupling further. This corresponds to the measurement schematic shown in Fig. 14. (β=39.81)

Parameter / Method	Q_o	Q_{ext}	Q_L	13 cell Nb Q_L
Q_{ext}	116371	2923	2851	38000
Q_L	116361	2922	2851	37997
Q_o	115913	2911	2840	37851
Average	116215	2919	2847	37950

From the data in Tables V-1 to V-5 the values of Q_o remain relatively constant, which should be expected since the losses in the cavity should remain constant and independent of the coupling. The inconsistencies are on the order of 1% and this is easily within the tolerances of

the results using FEM. Clearly, opening the beampipe on the cavity on the coupler-side of the cavity is critical for increasing the Q_L. To increase the coupling to a conservative level between the results obtained in Sec. V and Sec. IV, a moderate increase in beampipe diameter to 34 mm would result in a Q_L on the order of 2.5×10^6, while an increase in beampipe diameter to 38 mm results in a Q_L on the order of 1.5×10^5. This result could also be obtained with a 30 mm beampipe if in the region between the antenna and the cavity would be perturbed slightly. This opening could be done with regard to symmetry and polarizations while disturbing the cavity fields minimally. An example of this perturbation is presented in Figs. 15-16.

The geometries that were

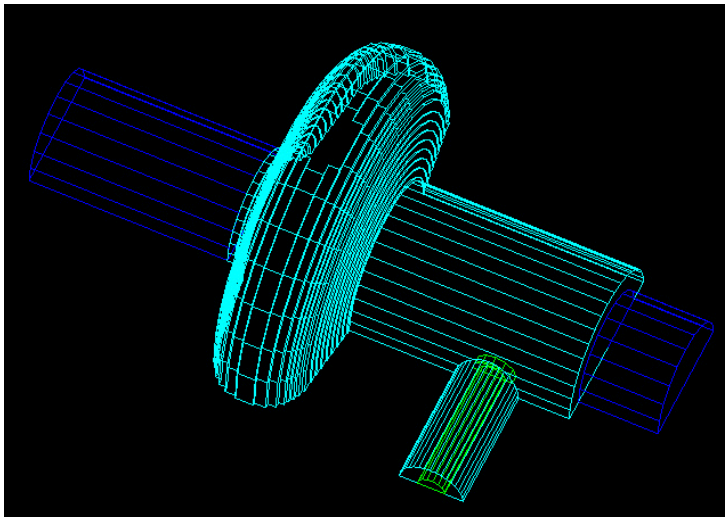

Figure 14. The 40 mm beampipe has a small hat added to it. The penetration is to the 30 mm beampipe.

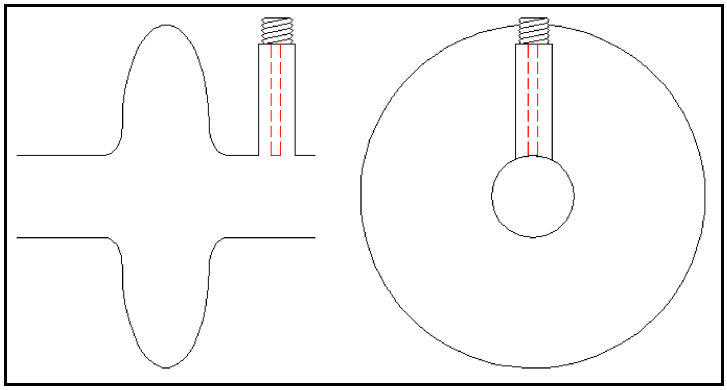

Figure 15. The original cavity layout - 30 mm beampipes and a simple E-probe coupler.

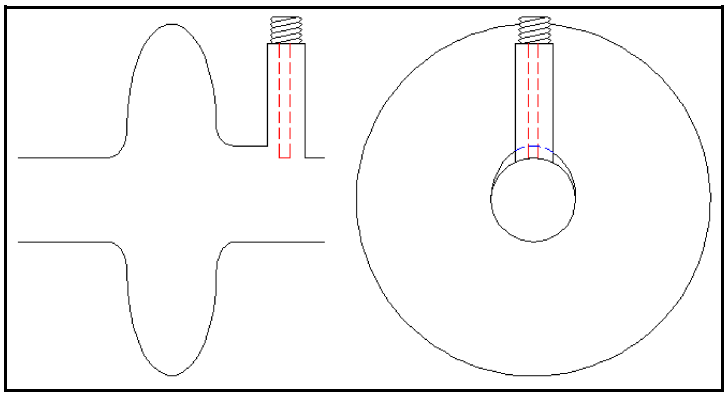

Figure 16. Model to increase coupling from Fig. 15. The region between the coupler and the input transmission line is modifies.

simulated in this section, namely in Figs. 13-14 are not necessarily the geometries that would be made in practice. The step discontinuity in beampipe on the opposite side of the coupler from the cavity is not something that would be made in practice. Rinsing procedures on the niobium would make this part difficult to keep clean. For the purposes of this simulation, however, this is acceptable since the fields evanesce and become a small component of energy storage in this vicinity. A proper discontinuity would be some sort of taper, whether it should be linear, exponential, or Gaussian in shape is a second order effect for the electromagnetics involved.

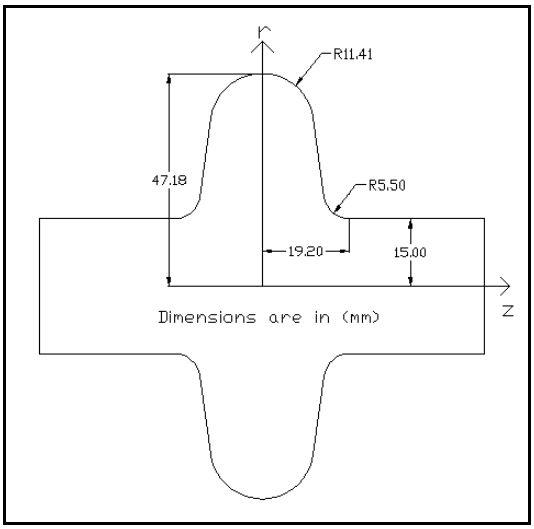

Figure 17. Cavity profile for the electromagnetic simulation.

VI. Meshing Considerations

For technical considerations, it is worth commenting upon how to set up the geometrical mesh for simulations within HFSS. Understanding how to take advantage of the meshing options available within HFSS allows one to substantially reduce simulation times without sacrificing accuracy of the results. The HFSS geometry model for the A0 cavity is discussed here in order to consider these meshing options while simultaneously documenting

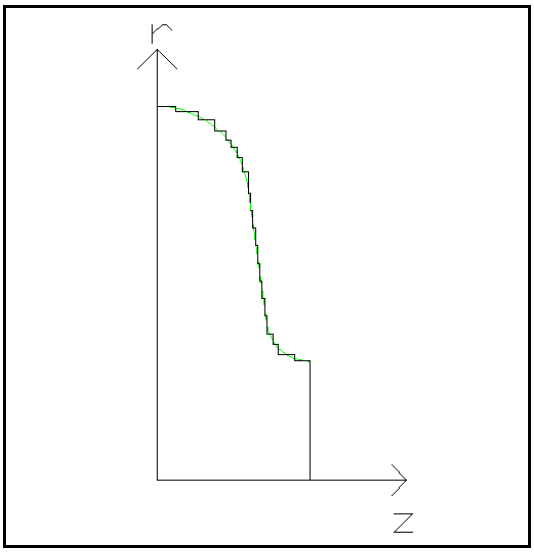

Figure 18. Discretized cavity profile.

some of the specific work required for generating this particular cavity geometry. The total simulation time achieved by using these meshing techniques was a factor of at least 4 less than not using these techniques.

To initiate the modeling, the cavity profile of Fig. 17, which is cylindrically symmetric about the z-axis, is discretized and modeled using cylinders of varying diameter and length. The discretized profile is depicted in Fig. 18 along with the actual profile. Only one-quarter of the cavity is shown for clarity. The actual cylinders used for creating the HFSS geometry are included in Table VI-1. This table represents half of the cavity since the other half is created using the mirroring function within HFSS.

Table VI-1. Cylinders used to create one-half of the cavity profile. All lengths are in millimeters.

Cylinder	Radius (mm)	Length (mm)
1	15.1	2.0
2	15.9	2.0
3	17.2	0.7
4	18.5	0.7
5	20.8	0.3
6	23.0	0.3
7	25.2	0.3
8	27.4	0.3
9	29.6	0.3
10	31.8	0.3
11	34.0	0.3
12	36.2	0.3
13	39.0	0.7
14	40.8	0.7
15	42.0	0.7
16	43.0	0.7
17	44.1	1.4
18	45.5	2.1
19	46.6	2.8
20	47.2	2.3

The length of the cylindrical beam pipe extending away from the cavity on both sides is chosen such that the first beam pipe mode has sufficiently evanesced at the beam pipe end, which is the boundary of the model geometry. This is important since HFSS assumes that all

created shapes are carved out of a perfectly conducting material. Thus choosing the beam pipe lengths with the aforementioned considerations ensures that the fields have been reduced to negligible magnitude at the reflective boundary of the beam pipe ends. This effectively simulates an infinite beam pipe and is valid since the operating frequency is below all beam pipe mode cutoff frequencies. In particular, the first beam-pipe mode is the TE_{11} mode whose cutoff frequency is calculated from,

$$f_{cutoff\ TE_{n,m}} = \frac{c_o \cdot \alpha_{n,m}}{2\pi a}$$

where $\alpha_{n,m}$ is the m[th] root of the equation , c_o is the velocity of light in vacuum, and a is the radius of the beam pipe. Thus, for beam pipe radii of 30mm and 40mm the TE_{11} cutoff frequency is 5.8GHz and 4.395GHz respectively. The associated guide wavelength is given as

where is the cutoff wavelength and is the free-space wavelength.

Furthermore, the TE_{11} beam pipe mode evanesces as where

Thus at the A0 cavity operating frequency of 3.9GHz, the TE_{11} 30mm beam pipe mode is attenuated by a factor of *e* for every 1.1 cm. The total beam pipe length placed on each side of the cavity was chosen to be 5 cm. Thus, any field at the cavity/beam pipe interface has attenuated to at least 1.06% at the model boundary, which translates to an attenuation of -39.5 dB.

To reduce simulation times and save on memory requirements, one can take advantage of the symmetry of the cavity/coupler geometry. The geometry and the cavity mode of interest are symmetric about a plane containing the cavity center and the line running down the center of the coupler. Thus, the HFSS model need only be a ½ model as depicted in Figure 19.

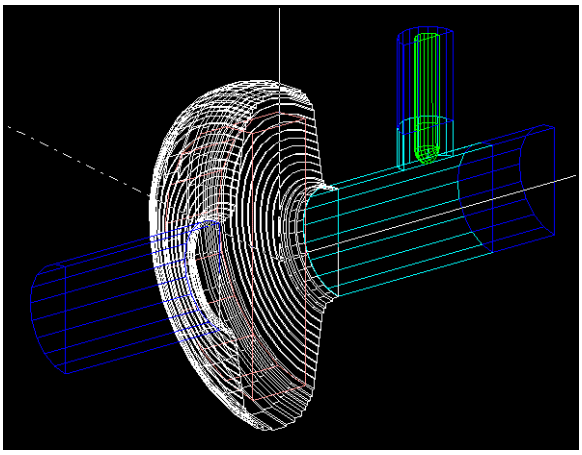

Figure 19. HFSS ½ model showing regions used to create a varying mesh.

To solve the problem correctly, the boundary condition at the cutting plane has to be set to a magnetic wall, forcing the appropriate symmetry condition for this particular problem. Furthermore, since only half of the input port is modeled, an impedance multiplier has to be used within HFSS in order to obtain the proper port impedance. This is evident from consideration of how the port impedance is calculated within HFSS. For a coaxial line, the characteristic impedance is calculated using the method outlined in Appendix A. Thus, when only ½ of the port is modeled, only ½ of the actual charge on the center conductor will be found when integrating along the surface of the modeled center conductor. Therefore, the capacitance value will be calculated as being ½ of its actual value, and consequently, the characteristic impedance will be calculated as being twice its actual value. Thus, to obtain the correct port impedance an impedance multiplier of 0.5 will bring the port impedance back to its actual value. This is a subtle but important detail to consider when taking advantage of symmetry conditions while simulating driven ports. Taking advantage of this symmetry reduces numerical noise, but also reduces the matrix equation to one-half of the dimension it would be otherwise. This roughly

reduces the solution time to one-fourth of the time it would take to solve the full problem.

To further reduce simulation overhead, the mesh is finely controlled using the available meshing options within HFSS. The required size of the mesh elements is basically dependent upon how the fields are varying spatially, which in turn is dependent upon the operating frequency and the geometry of the problem. In areas relatively far from discontinuities, only propagating modes can exist, and thus knowledge of the associated wavenumbers gives one an idea on how the fields vary spatially. In areas containing discontinuities, the field will vary more rapidly and thus the mesh size elements need to be finer in these areas than in areas not containing discontinuities.

When HFSS meshes a geometry, it initiates its mesh with an element size based upon the free-space wavelength associated with the operating frequency and/or a user defined seeding operation. The seeding operation allows a user to define a maximum element length with the option of placing a limit on the maximum number of mesh elements.. It then performs a user

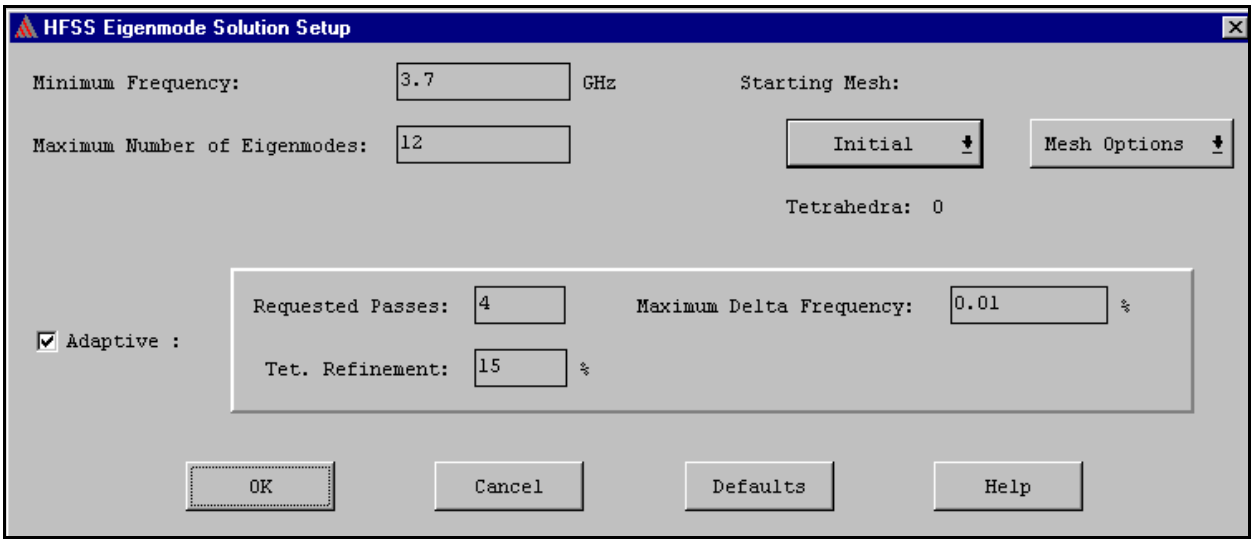

Figure 20. HFSS eigenmode solution setup dialog box.

specified number of adaptive mesh refinements, refining the mesh at each step by a user defined percentage. The success of the mesh can be measured by first performing an eigenmode solution and looking at the delta-frequency change in the calculated eigenmode resonant frequencies. For this particular problem, the mesh settings were optimized to achieve a maximum delta-frequency of 0.01% for the first 12 eigenmodes. The HFSS setup screen showing the eigenmode solution settings is shown in Fig. 20.

One of the tricks used in meshing the problem included creating a cylinder within the cavity region. This cylinder is the orange cylinder (which is somewhat hidden within the white cavity region) shown in Fig. 19. The mesh within this cylinder was set to a coarser mesh than the volume between this cylinder and the white boundary of the cavity profile. Furthermore, the dark

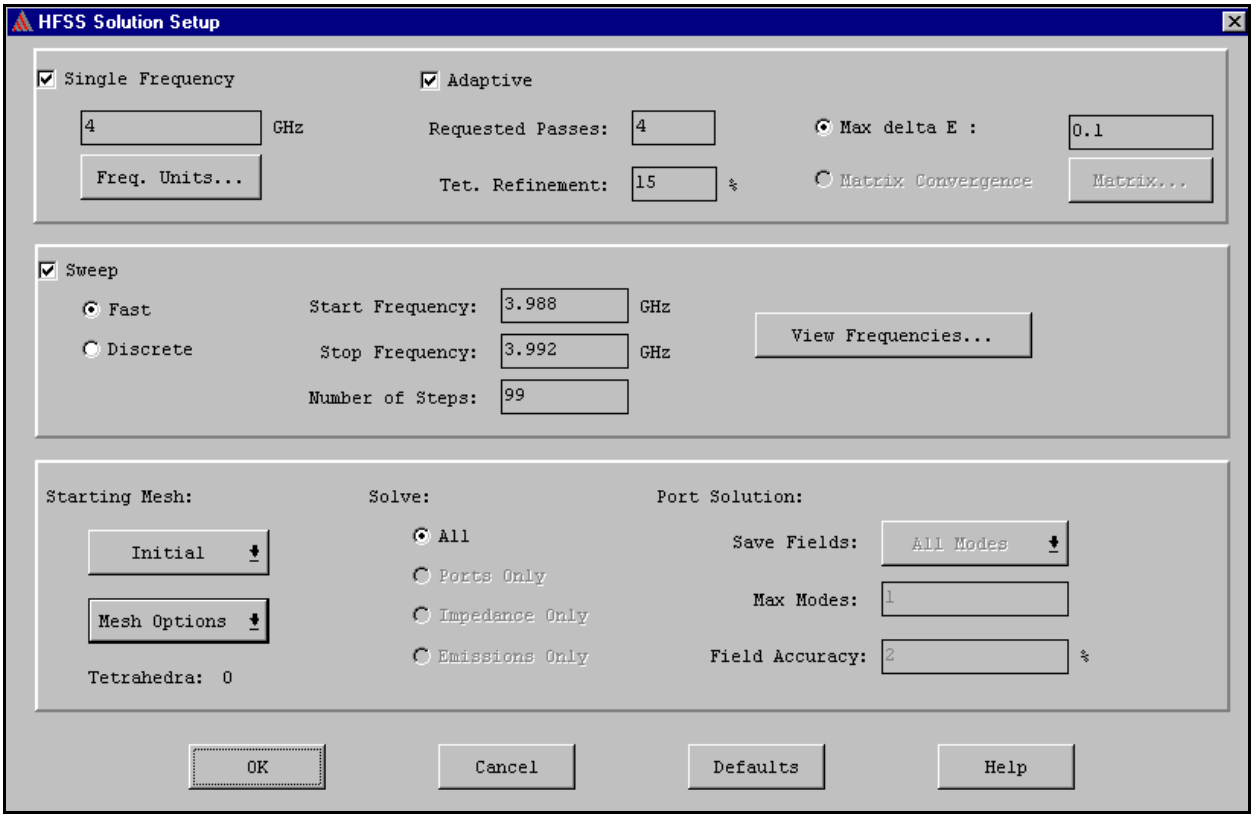

Figure 21. HFSS driven solution setup box.

blue beampipes used this same coarser mesh while the light blue regions, including the coupler/beam pipe interface, used the same finer mesh as that used for volume between the cavity profile and the orange cylinder. A fine mesh is necessary to accommodate the energy storage around the cavity walls, but within the cavity, it is not necessary to have a fine mesh since its energy storage and fields can be easily expanded in large tetrahedra.

Once the mesh settings have been verified to give confident results, a driven solution is performed. The same initial mesh options are used with the driven solution as well as the same number of requested passes with the same percentage refinement. The only subtlety with the driven solution is to set the initial single frequency at which the mesh refinement takes place to a frequency above the maximum frequency sweep limit. Figure 21 shows example settings.

VII - Conclusion

Use of FEM codes to predict the Q's of cavities can be straightforward using the definitions of each particular Q. The results of most quality factors are as predicted, although some Q-factors seem to have numeric error associated with them, whether the numeric error is density of mesh, or the coupler is critically coupled, or severely undercoupled. A thorough design review of the coupler should include couplers that are non-50Ω, waveguide, and couplers that have a flared beampipe and are openly exposed to the cavity. Couplers that are straight E-probes and are flush with the beampipe all have relatively identical coupling. While this coupling is below the design criteria, the simulations are not perfect and the mesh must be extremely tight in the vicinity of the coupler to exactly trust the results to within one millimeter. Based on the results presented in this paper, either an off-axis coupler should be considered with

the use of a hat, or the beampipe will need to be opened. Use of the off-axis antenna and hat combination provides a factor of 4 better than what is required. While this provides a level of electromagnetic/system design comfort, the antenna configuration may undergo strong multipactoring. Opening the beampipe strongly influences the Q_L and this is probably the cheapest and quickest alternative for a conservative and robust design given the data researched so far.

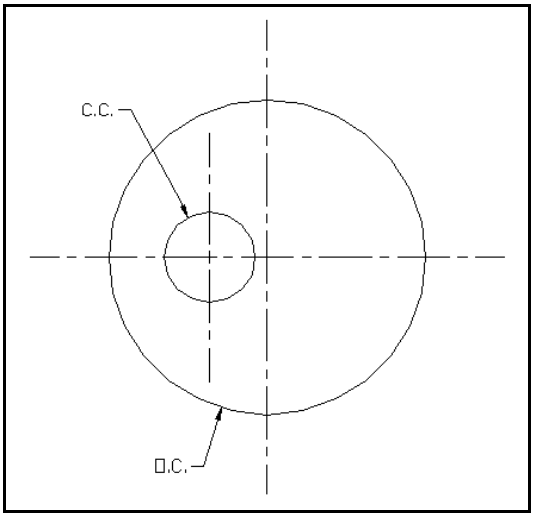

Figure 22. The center conductor is shifted off-axis from the outer conductor. It is desired to know the characteristic impedance of this geometry.

Appendix A - Calculation of Off-Axis Transmission Line Impedance

It is desired to calculate the characteristic impedance of an off-axis transmission line. This is represented pictorially by Fig. A-1. This problem can be solved easily using introductory transmission line theory. The first step is to solve Laplace's equation subject to the boundary condition:

This equation can be solved using any number of finite element programs. After finding $\varphi\left(\vec{r}\right)$, it is then necessary to find the electric field via the relationship:

$$\vec{E}\left(\vec{r}\right) = -\nabla\varphi\left(\vec{r}\right).$$

The charge density on the center conductor is therefore $\varepsilon_r\varepsilon_o\vec{E}\left(c.c.\right)\cdot\hat{n} = \rho_s\left(\vec{r}\right)$, and $\varepsilon_r\varepsilon_o\vec{E}\left(o.c.\right)\cdot\hat{n} = -\rho_s$ where the fields are evaluated on the surface of the conductors, and $\hat{n}$ is the outward pointing normal vector from the surface of c.c. The total charge is then found by

integrating along the surface of the center conductor:

$$Q = \varepsilon_r \varepsilon_o \oint_{c.c.} \vec{E} \cdot \hat{n} dl.$$

The capacitance per unit length is therefore found by Q=CV→C=Q because V=1 V. We assume that $\varepsilon_r = \mu_r = 1,$ and the inductance per unit length can be calculated by the speed of light:

$$c_o = \frac{1}{\sqrt{LC}} \Rightarrow L = \frac{1}{c_o^2 C}.$$

The characteristic impedance is then

$$R_o = \sqrt{\frac{L}{C}} = \frac{1}{c_o C}.$$